ADVANCED MATERIALS
www.advmat.de

A Low-Temperature, Solution-Processable, Cu-Doped Nickel Oxide Hole-Transporting Layer via the Combustion Method for High-Performance Thin-Film Perovskite Solar Cells

*Jae Woong Jung, Chu-Chen Chueh, and Alex K.-Y. Jen**

The promising photophysical properties of the emerging organometallic halide perovskites, such as intense broadband absorption, high charge carrier mobility, and long charge diffusion length, have enabled the rapid development in solar cells reaching over 20% power conversion efficiency (PCE) recently.[1] Especially, the low material cost and facile solution processability of perovskites are very attractive as next-generation photovoltaic materials for sustainable energy.

In general, the perovskite-based solar cells (PVSCs) consist of methylammonium lead halide perovskite ($CH_3NH_3PbX_3$, X = Br^-, Cl^-, or I^-) as the photoactive layer sandwiched by charge-transporting interlayers (CTLs) and corresponding electrodes. Among many device architectures that have been developed so far for PVSCs, the planar heterojunction (PHJ) configuration has unique advantages due to its relatively low-temperature solution processing compared to the conventional transition metal oxide (TMO)-based mesosuperstructures that requires high-temperature sintering (>450 °C).[2] However, limited by the smaller interfacial area between the perovskite absorber and the CTLs in the PHJ geometry than the mesosuperstructure scaffold, proper selection of CTLs is very important for achieving high photovoltaic performance.[3]

In principle, an ideal CTL for highly efficient PVSCs needs to meet the following requirements: (i) good optical transparency, (ii) decent electrical conductivity, (iii) efficient charge-transporting/blocking capability, (iv) low-temperature solution processability, and (v) suitable surface energy for perovskite crystal growth, especially in the conventional device configuration. Both organic and inorganic semiconductors have been extensively exploited for their suitability in fabricating PHJ PVSCs.[4] For the organic hole-transporting layer (HTL), conducting poly(3,4-ethylene dioxythiophene):poly(4-styrenesulfonate) (PEDOT:PSS) is one the most commonly used HTLs in the PHJ PVSCs.[5] Very promising PCE of over 15% has been demonstrated; however, its hydroscopic and acidic nature significantly impede the further improvements on device stability.

Dr. J. W. Jung, Dr. C.-C. Chueh, Prof. A. K.-Y. Jen
Department of Materials Science and Engineering
University of Washington
Seattle, WA 98195, USA
E-mail: ajen@u.washington.edu
Prof. A. K.-Y. Jen
Department of Chemistry
University of Washington
Seattle, WA 98195, USA

DOI: 10.1002/adma.201503298

In this regard, solution-processed inorganic counterparts with high transparency and appropriate work functions (WFs) are promising alternatives for high-performance PHJ PVSCs. Thus far, various inorganic materials such as CuSCN, NiO, and V_2O_5 have been introduced as efficient HTLs in the PHJ PVSCs,[6a–d] and promising photovoltaic performance has been achieved. Recently, our group also has demonstrated that the potential of the p-type CuSCN serving as a promising HTL to achieve high-performance PHJ PVSCs via facile solution process.[6e] Another interesting class of p-type semiconductor is nickel oxide (NiO_x). NiO_x interlayer has shown great promise as HTL due to its intrinsic p-type semiconducting nature, high optical transmittance, and deep-lying valence band (VB of 5.4 eV) that matches well with the VB of $CH_3NH_3PbI_3$.[7a,b] Very respectable PCE (9%–11%) based on sol–gel-derived NiO_x HTLs have been reported for PHJ PVSCs, revealing their potential for achieving high-performance devices.[7c–f]

More recently, light Cu-doped NiO_x HTL with significantly enhanced electrical conductivity has been shown by Jen et al. to improve the performance of PHJ devices from 8.9% to 15.4%. This encouraging result shows the promise of using Cu-doped NiO_x (Cu:NiO_x) as an excellent HTL for PHJ PVSCs.[8] However, the Cu:NiO_x HTL prepared by the sol–gel method needs to be annealed at high temperatures above 400 °C in order to achieve high crystallinity. This high-temperature process not only will increase the cost of device fabrication but also create incompatibility with commonly used polymer substrates for roll-to-roll printings. Based on these limitations, it is imperative to develop a suitable method that can process Cu:NiO_x HTL at lower temperatures for PHJ PVSCs.

Recently, combustion chemistry has been reported as a feasible route to prepare high crystallinity solution-processed TMO thin films at much lower temperatures than those used for traditional sol–gel process.[9] Its unique self-energy generation and exothermic reaction provide a lower transition energy to drive the formation of the TMO lattices, avoiding the need for high thermal energy. This allows lower processing temperature to be used to replace sol–gel reactions that are endothermic which requires significant external thermal energy to form TMO lattices and remove organic impurities. Lately, various TMO thin films have been successfully prepared via such combustion method at relatively low temperatures.[10]

One of the interesting examples is the one reported by Mark et al. demonstrating high-performance thin-film transistors using combustion processed indium oxide at 200 °C.[11] In addition to achieving high-performance thin-film transistors, the combustion-processed TMOs have also been explored as efficient HTLs for fabricating organic solar cells, validating this

© 2015 WILEY-VCH Verlag GmbH & Co. KGaA, Weinheim

method's strong potential as a novel low-temperature, solution-processed route for preparing TMO-based HTLs.[12]

Here, we report the successful development of a low-temperature (150 °C), solution-processable Cu:NiO_x via the combustion method and its use as an excellent HTL for PHJ PVSCs. The Cu:NiO_x thin films prepared from this combustion route possess both homogeneous morphology and high crystallinity. More importantly, it exhibits better photoluminescence (PL) quenching efficiency with the $CH_3NH_3PbI_3$ absorber than that uses conventional sol–gel method prepared Cu:NiO_x. This indicates its respectable hole extraction/collection capability. As a result, PHJ PVSC with this low-temperature-processed Cu:NiO_x affords an impressive PCE of 17.74%, outperforming that based on high-temperature-processed Cu:NiO_x (PCE = 15.52%).

Furthermore, this low-temperature-processed Cu:NiO_x enables the fabrication of ITO-free PVSC with impressive PCE (as high as 13.4%), which signifies its general applicability for a variety of substrates and electrodes. This work reveals not only the great potential for preparing low-temperature-processed Cu:NiO_x HTL, but also represents an important step for achieving high-performance PHJ PVSCs.

As shown in our previous work, Cu:NiO_x prepared via the conventional sol–gel process involves the use of nickel acetate and copper acetate as precursors at 500 °C.[8] For the combustion-reaction-based Cu:NiO_x thin films, nickel nitrate hexahydrate and acetylacetone were used as oxidizer and fuel, respectively (**Figure 1**a). The similar 5 mol% copper nitrate trihydrate was added as dopant to improve the overall electrical conductivity. The combustion reaction for preparing Cu:NiO_x was monitored by using differential scanning calorimetry (DSC) and thermogravimetric analysis (TGA). As shown in Figure 1b, the prepared Cu:NiO_x exhibits an intense exothermic peak at ≈130 °C in the DSC curve, which coincides well with the abrupt mass loss temperature at ≈130 °C shown in TGA curve. This implies that the formation of Cu:NiO_x via combustion reaction can be effectively driven at a much lower temperature. The results from UV–vis absorption spectra and X-ray diffraction (XRD) also verify the formation of combustion-derived Cu:NiO_x, as shown in Figure S1 in the Supporting Information. Note that the threshold temperature for this combustion reaction is above 130 °C since a lower temperature, i.e., 100 °C cannot initiate the combustion reaction effectively. The X-ray photoelectron spectroscopy (XPS) shown in Figure S2 (Supporting Information) reveals that the Cu was successfully incorporated in NiO_x in its divalent state, which is quite similar to case obtained by conventional sol–gel process. As a result, both Cu:NiO_x films exhibit similar work function of −5.3 eV, as estimated by ultraviolet photoemission spectroscopy (Figure S3, Supporting Information). In order to ensure the formation of highly crystalline Cu:NiO_x, this combustion reaction was performed at 150 °C in this study and the details for Cu:NiO_x preparation was described in the Experimental Section.

To examine the quality of the prepared $CuNiO_x$ thin film, its crystallinity and transmittance have been characterized and compared with the Cu:NiO_x films prepared by the conventional sol–gel process. As shown in **Figure 2**a, both Cu:NiO_x films prepared by sol–gel and combustion methods exhibited distinct diffractions with comparable intensities at $2\theta = 37.8°$ and 43.7°, representing the typical diffraction peaks of (111) and (200) planes for the cubic-structured NiO.[12b] In addition, the transmittance of both Cu:NiO_x films depicted in Figure 2b showed resembling spectra, where the absorption of the precursors at long wavelength region (700–1000 nm) was clearly diminished. These results affirm the formation of well-grown NiO_x crystals from the low-temperature combustion process. It is interesting to note that the combustion-derived Cu:NiO_x film showed higher optical transparency in the region between 600 and 950 nm than that prepared by the conventional sol–gel process. The distinct absorption in the long wavelength region of the Cu:NiO_x films prepared by different methods is mainly attributed to their different degree of nickel vacancies.[7b] This region coincides partially with the absorption of $CH_3NH_3PbI_3$, which can enable the combustion-derived Cu:NiO_x HTL to absorb more light in this region to enhance device's photocurrent.

The surface morphology of the combustion-derived Cu:NiO_x film was examined by atomic force microscopy (AFM) (Figure S4, Supporting Information). The combustion-derived Cu:NiO_x at 150 °C clearly exhibits a smooth and compact surface morphology (RMS roughness = 4.5 nm) which is comparable to that prepared by the sol–gel method (RMS roughness = 5.8 nm). Very impressively, the combustion-derived Cu:NiO_x film possesses an almost twofold higher electrical conductivity (1.25×10^{-3} S cm^{-1}) than that of high-temperature-processed film (7.54×10^{-4} S cm^{-1}) as measured by the four-point probe measurement, indicating the Cu:NiO_x film prepared by such low-temperature combustion method can still maintain respectable crystallinity. All these results support the great advantages of using the combustion method over the conventional sol–gel method for preparing Cu:NiO_x HTLs.

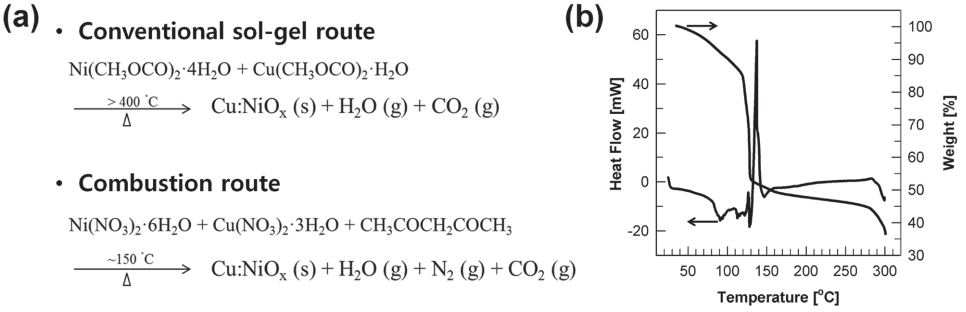

Figure 1. a) Depiction of the synthetic routes for Cu:NiO_x and b) DSC and TGA curves of the prepared Cu:NiO_x via the combustion process.

© 2015 WILEY-VCH Verlag GmbH & Co. KGaA, Weinheim
Adv. Mater. **2015**,
DOI: 10.1002/adma.201503298

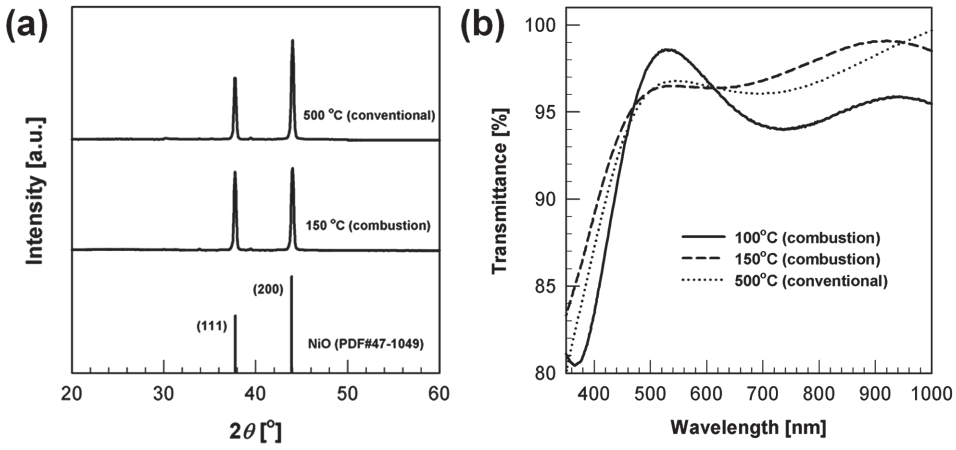

Figure 2. a) XRD diffractograms and b) transmittance spectra of the Cu:NiO_x films prepared through combustion and conventional methods.

It has been documented that perovskite film morphology, such as surface coverage, crystallinity, and roughness, is pivotal for photovoltaic performance of the derived devices.[13] To understand the perovskite film formation on top of the combustion-derived Cu:NiO_x layer, field-effect scanning electron microscopy (FE-SEM) and XRD were employed to examine the formed perovskite layer and the relevant results were presented in **Figure 3**a,b. In order to obtain a high crystallinity $CH_3NH_3PbI_3$ thin-film, we have adopted the one-step spin-coating method with toluene washing in this study to deposit this layer, which can facilitate rapid and homogeneous nucleation of perovskites.[14]

As can be clearly seen, the $CH_3NH_3PbI_3$ film grown on the combustion-derived Cu:NiO_x film exhibits a fully covered surface morphology with well-crystallized and densely packed grains, which is similar to that formed on the high-temperature-processed Cu:NiO_x. Moreover, the perovskite film grown on

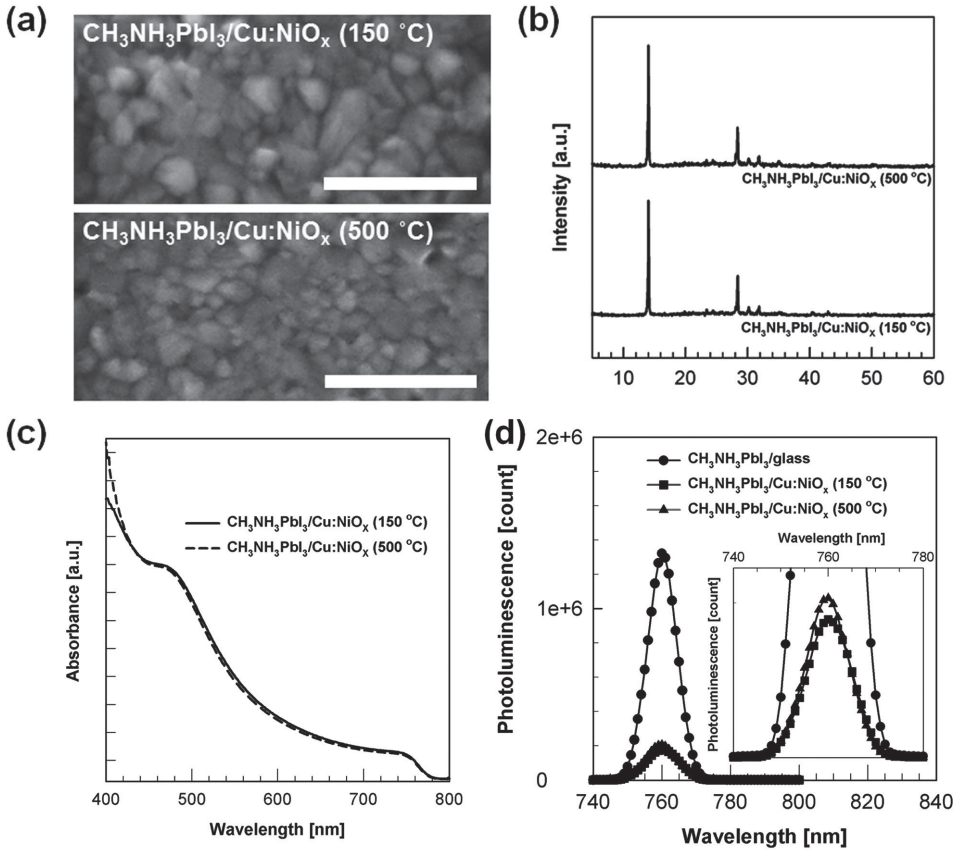

Figure 3. a) SEM images (scale bar = 1 μm), b) XRD diffractograms, c) UV–vis absorption spectra, and d) PL spectra of the $CH_3NH_3PbI_3$ films grown on Cu:NiO_x films prepared through combustion and conventional methods.

© 2015 WILEY-VCH Verlag GmbH & Co. KGaA, Weinheim

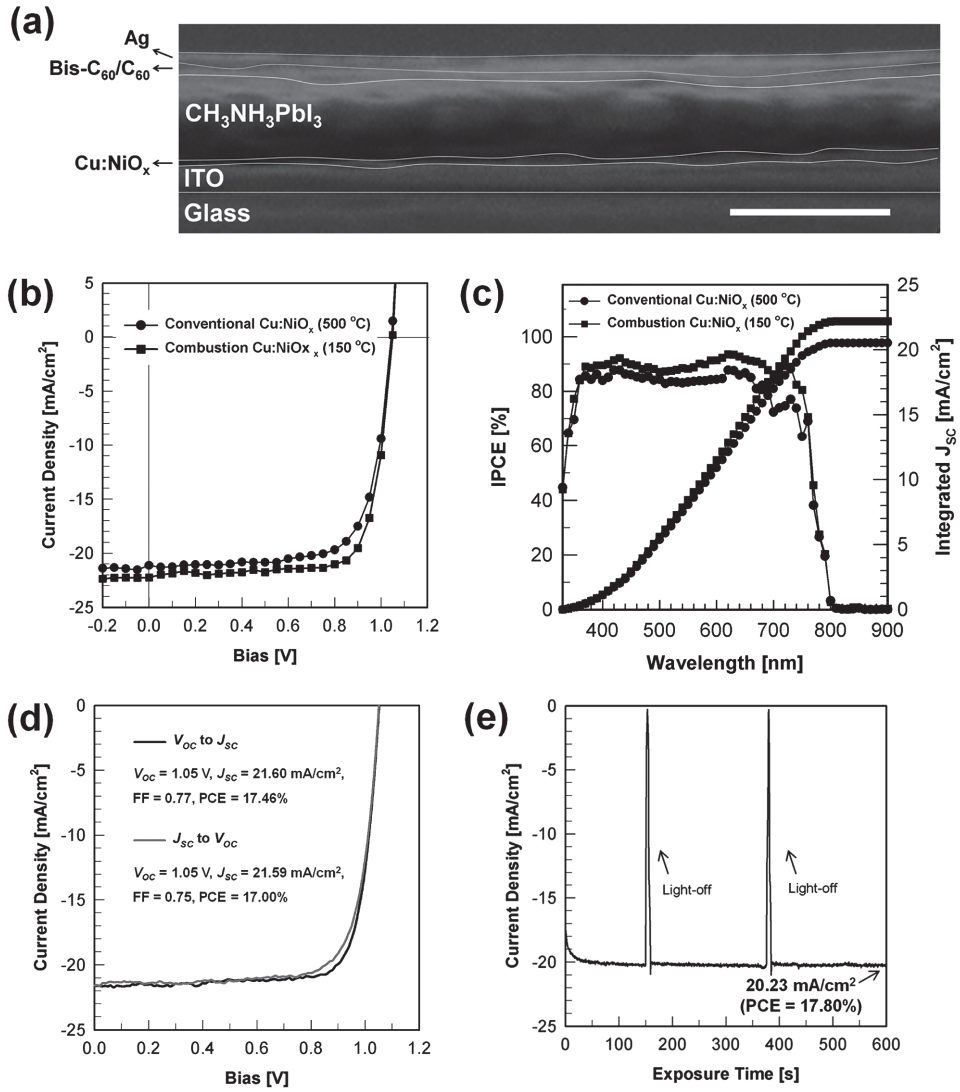

Figure 4. a) Cross-sectional FE-SEM image of the complete solar cell device (scale bar = 500 nm), b) *J–V* curves, and c) IPCE spectra of the device-based Cu:NiO_x as hole-transporting layers prepared through different methods. d) *J–V* curves with different scan directions, and e) steady-state photocurrent density at 0.88 V of bias for 10 min under continuous light illumination of the device with combustion-derived Cu:NiO_x HTL.

the combustion-derived Cu:NiO_x shows a larger average grain size (300–500 nm) than that (100–300 nm) grown on the high-temperature-processed Cu:NiO_x. This can be attributed to the different surface morphologies of the studied Cu:NiO_x films as shown in Figure S4 in the Supporting Information. The XRD spectra of both perovskite films exhibit comparable intensities of diffraction signals at 13.95° and 28.35°, corresponding to the (110) and (220) planes of tetragonal $CH_3NH_3PbI_3$ phase. In addition, the UV–vis absorption spectrum of the perovskite film grown on the combustion-derived Cu:NiO_x was identical to that of the perovskite film grown on high-temperature-processed Cu:NiO_x (Figure 3c), indicating that highly crystalline perovskite films are grown on Cu:NiO_x films regardless of the different preparation routes.

The charge extraction efficiency of the combustion-derived Cu:NiO_x film was elucidated by steady-state PL quenching experiment with the perovskite film on top of it. As represented in Figure 3d, the $CH_3NH_3PbI_3$ film shows even more efficient PL quenching on the combustion-derived Cu:NiO_x film than that from the sol–gel-derived Cu:NiO_x film, suggesting its enhanced hole extraction and transport as a result of the improved electrical conductivity as discussed earlier.

To investigate the efficacy of the combustion-derived Cu:NiO_x HTL in PHJ PVSCs, the solar cell devices were fabricated with the configuration of ITO/Cu:NiO_x/$CH_3NH_3PbI_3$/C_{60}/Bis-C_{60}/Ag (**Figure 4**a). The detailed fabrication procedures for the devices were described in the Experimental Section. The optimized thickness and annealing temperature of the combustion-derived Cu:NiO_x HTL in the device were 50 nm and 150 °C, respectively (see Table S1 and S2 in the Supporting Information). It is worth to note that the electron-transporting layer (ETL) used herein is C_{60} instead of $PC_{61}BM$ due to its superior mobility.[15] Figure 4b presents the *J–V* curves of the fabricated PVSCs based on two different Cu:NiO_x layers for comparison

© 2015 WILEY-VCH Verlag GmbH & Co. KGaA, Weinheim
Adv. Mater. **2015**,
DOI: 10.1002/adma.201503298

Table 1. Device parameters of the PvSCs with Cu:NiO_x HTL prepared through combustion and conventional sol–gel methods.

Process for Cu:NiO_x	V_{OC} [V]	J_{SC} [mA cm^{-2}]	FF	PCE[a)] [%]	R_s [Ω cm^{-2}]	R_{sh} [10^3 Ω cm^{-2}]
Combustion	1.05	22.23	0.76	17.74 (17.30)	1.8	3.9
Conventional sol–gel	1.05	20.53	0.72	15.52 (15.14)	3.7	3.1

[a)]Average PCE in bracket (over 12 devices).

and the relevant parameters and statistic results are summarized in **Table 1** and Figure S5 in the Supporting Information. Very encouragingly, the PVSC based on the combustion-derived Cu:NiO_x HTL exhibits an promising PCE of 17.74% with a V_{OC} of 1.05 V, a J_{SC} of 22.23 mA cm^{-2}, and an FF of 0.76, outperforming the performance of the device derived from the conventional high-temperature-processed Cu:NiO_x HTL (V_{OC}, J_{SC}, FF, and PCE are 1.05 V, 20.53 mA cm^{-2}, 0.72, and 15.52%, respectively).

The major improvement lies on the increased J_{SC} and FF, which can be attributed to the improved charge extraction/collection of the combustion-derived Cu:NiO_x as a result of enhanced electrical conductivity compared to that prepared by the conventional sol–gel method. The reduced series resistance (R_s) and increased shunt resistance (R_{sh}) of the device using combustion-derived Cu:NiO_x HTL imply that its increased electrical conductivity facilitates more efficient charge transport and collection from the perovskite layer (see Table 1). It is noteworthy that the devices exhibited very small dependency on the thickness of Cu:NiO_x within 100 nm and a high PCE of over 15% can be still remained when a 150 nm thick Cu:NiO_x HTL is used in the device (Table S2, Supporting Information), revealing the superior charge transporting property of such combustion-derived Cu:NiO_x HTL. To further investigate the charge transport and recombination behaviors in device, their electrochemical impedance spectroscopy was studied over the frequency range between 0.1 Hz and 5 MHz under illumination at a constant bias of 150 mV. As shown in Figure S6 in the Supporting Information, both devices using conventional and combustion-derived Cu:NiO_x HTL exhibit the typical Niquist plots. Because the high and low frequencies of the PVSCs are relatively correlated with the hole transport (extraction) at the HTL/electrode interface and the charge recombination within perovskite and at the interface of perovskite/CTLs, respectively, the plots can be fitted using a simple equivalent circuit model including series resistance (R_s), recombination resistance (R_{rec}), and HTL resistance (R_{HTL}) (see the insert in Figure S6 in the Supporting Information).[16] As a result, the R_s of the device based on combustion-derived Cu:NiO_x (8 Ω) is significantly lower than that of the device using the sol–gel-derived Cu:NiO_x (28 Ω), indicating that improved conductivity of HTL reduces the contact resistance at perovskite/HTL interface. More importantly, the device using combustion-derived Cu:NiO_x also exhibits an increased R_{rec} (355 Ω) as compared to that of the device using the sol–gel-derived Cu:NiO_x (R_{rec} = 284 Ω). The lower R_{rec} suggests that the combustion-derived Cu:NiO_x HTL enables a lower recombination rate in device than that of the sol–gel-derived Cu:NiO_x.[4c] Furthermore, the lower R_{HTL} of the device employing combustion-derived Cu:NiO_x HTL (658 Ω) than the one based on the sol–gel-derived Cu:NiO_x HTL (1025 Ω) also confirms that improved charge transport of the former as a result of the increased conductivity. The impedance analysis clearly demonstrates that the PVSC using a combustion-derived Cu:NiO_x HTL results in reduced charge recombination in device compared to the sol–gel-derived Cu:NiO_x HTL to further enhance photovoltaic performance.

Shown in Figure 4c are the incident photon-to-current density efficiency (IPCE) spectra of the studied devices, in which the J_{SC}s of the devices integrated from the IPCE spectra match well with those obtained in the *J–V* measurements. The markedly improved IPCE in long wavelength region (620–780 nm) coincides well with the enhanced transmittance of the combustion-derived Cu:NiO_x film discussed earlier. This shows the importance of improved HTL optical transparency in enhancing the J_{SC} of derived devices.

The hysteresis of *J–V* curves in the PVSCs has been frequently mentioned as a serious concern that can potentially overestimate device's actual photovoltaic performance, especially for the planar geometry devices.[17] To clarify this issue, the hysteresis of the device employing the combustion-derived Cu:NiOx HTL was investigated. As shown in Figure 4d, the derived device exhibits a subtle discrepancy between its forward (PCE = 17.00%) and backward (PCE = 17.46%) *J–V* measurement where the average PCE from the continuous forward and backward *J–V* curves was 17.24% (V_{OC} = 1.05 V, J_{SC} = 21.60 mA cm^{-2}, and FF = 0.76).

To further verify the reliability of the device performance, we have performed the steady state photocurrent generation experiment at the maximum power point under illumination. As shown in Figure 4e, the device using combustion-derived Cu:NiO_x HTL shows a stabilized photocurrent of ≈20.2 mA cm^{-2} when it is biased at 0.88V under the continuous illumination for 10 min, which is in good agreement with the value obtained from the *J–V* measurements. Moreover, the final current density of 20.23 mA cm^{-2}, which is corresponding to a PCE of 17.80%, also agrees well with the value obtained from the *J–V* measurements. In addition, five different devices made from independent batches exhibit almost the same photovoltaic performance (Figure S7 and Table S2, Supporting Information), revealing the high reproducibility of the devices derived from the combustion-derived Cu:NiO_x HTLs.

By taking advantage of the low-temperature combustion reaction, we have further fabricated ITO-free PHJ PVSCs utilizing highly conductive PEDOT:PSS as the transparent anode. The limiting factor for the conductive PEDOT:PSS electrode lies on its much lower degradation temperature compared to that of the typical ITO electrode. In this regard, it is imperative to develop a low-temperature-processed HTL to construct ITO-free devices. The low-temperature combustion-derived Cu:NiO_x HTL is an ideal system to be combined with the highly conductive PEDOT:PSS electrode for fabricating high-performance ITO-free PHJ PVSCs. The detailed information for preparing highly

© 2015 WILEY-VCH Verlag GmbH & Co. KGaA, Weinheim

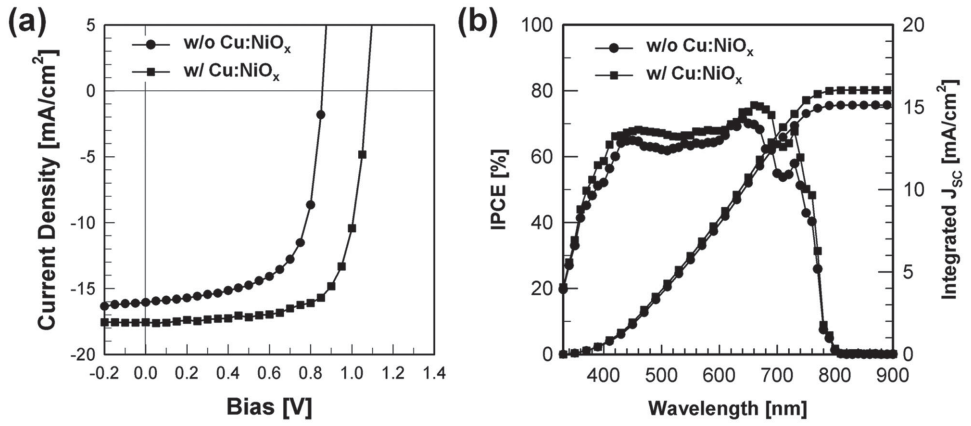

Figure 5. a) *J–V* curves and b) IPCE spectra of ITO-free PHJ PVSCs with and without combustion-derived Cu:NiO_x HTL.

conductive PEDOT:PSS electrode and device fabrication for the ITO-free PVSCs are described in the Supporting Information. The low-temperature combustion process enables the successful formation of Cu:NiOx HTL on top of the transparent PEDOT:PSS electrode, as shown in Figure S8 in the Supporting Information. **Figure 5**a shows the *J–V* curves of the ITO-free PVSC devices. The ITO-free device using Cu:NiO_x HTL exhibits a much enhanced PCE of 13.42% (V_{OC} = 1.05 V, J_{SC} = 17.75 mA cm^{-2}, FF = 0.72) compared to that without using Cu:NiO_x (PCE = 8.83%, V_{OC} = 0.86 V, J_{SC} = 16.05 mA cm^{-2}, FF = 0.64). The IPCE spectra of the devices in Figure 5b also clearly shows the efficient photo-generated charge collection at electrodes when combined with Cu:NiO_x HTL in spite of the lower optical transmittance introduced by this layer, indicating its good compatibility with the conductive polymer electrode for making ITO-free PVSCs.

In conclusion, we have demonstrated that low-temperature combustion process is a very efficient solution-derived method for preparing Cu:NiO_x HTL for high-performance PHJ PVSCs. In spite of its reduced processing temperature, the crystallinity, homogeneity, optical transparency, and electrical conductivity of the Cu:NiO_x film prepared from this combustion process are comparable or even better than those prepared from the conventional high-temperature sol–gel process. The resulting PHJ PVSC exhibits a very high PCE up to 17.8%, which outperforms that of the control device using the high-temperature sol–gel-derived Cu:NiO_x HTL. In addition, this unique low-temperature process enables an ITO-free PVSC to be fabricated to achieve an impressive PCE of 13.4%, signifying its excellent applicability for a variety of substrates and electrodes. All these results clearly reveal the efficacy of combustion method for fabricating high quality Cu:NiO_x HTL for high-performance PHJ PVSCs.

Experimental Section

Materials and Sample Preparation: For the combustion-derived Cu:NiO_x, 276.3 mg of $Ni(NO_3)_2{\cdot}6H_2O$ (0.95 mmol) and 12.1 mg of $Cu(NO_3)_2{\cdot}3H_2O$ (0.05 mmol) were dissolved in 2-methoxyethanol (10 mL). After the solution was stirred at 50 °C for 1 h, 10 µL of acetylacetone was added to the solution, and the solution was further stirred for 1 h at room temperature. The Cu:NiO_x from conventional high-temperature process was prepared as reported elsewhere. To prepare the perovskite precursor solution, CH_3NH_3I and PbI_2 (Alfa Aeser) were dissolved in mixed solvent of dimethylsulfoxide and γ-butyrolactone (3:7 in volume) in 1 M concentration, and then stirred at 70 °C for 1 h. All the solutions were filtered with 0.45 µm PVDF filters before spin-coating.

Fabrication of Thin-Film Perovskite Solar Cells: The ITO-coated glass substrates (15 Ω sq^{-1}) were cleaned sequentially with detergent and deionized water, acetone, and isopropanol under sonication for 30 min, and then the substrates were treated with O_3-plasma for 60 s. After Cu:NiO_x layer was formed by spin-coating onto the ITO-coated glass, the substrate was annealed in ambient atmosphere for 1 h at 150 °C and 500 °C for combustion and conventional process, respectively. After the substrates were cooled to RT, the perovskite layer was formed by spin-coating the precursor solution at 5000 rpm for 45 s. After 25 s, 80 µL of toluene was poured on top of the substrates during spin-coating which is a slightly modified method from the reported protocol.[14] After thermal annealing at 100 °C for 10 min, the C_{60} (15 mg mL^{-1} in *o*-DCB) and bis-C_{60} surfactant (2 mg mL^{-1} in isopropyl alcohol) were then sequentially deposited by spin-coating at 1200 rpm for 60 s and 3k rpm for 60 s, respectively. Finally, 120 nm of Ag was evaporated under high vacuum (<2 × 10^{-6} Torr). The device area was defined by the shadow mask as 3.14 mm^2. All the *J–V* curves in this study were recorded using a Keithley 2400 source meter. The device photocurrent was measured under AM1.5 illumination condition at an intensity of 100 mW cm^{-2}. The illumination intensity of the light source was accurately calibrated with a standard Si photodiode detector equipped with a KG-5 filter, which can be traced back to the standard cell of the National Renewable Energy Laboratory (NREL). The hysteresis of the *J–V* curves was recorded at 100 mV s^{-1}. The IPCE spectra of the device were obtained from an IPCE setup consisting of a Xenon lamp (Oriel, 450 W) as the light source, a monochromator, a chopper with a frequency of 100 Hz, a lock-in amplifier (SR830, Stanford Research Corp), and an Si-based diode (J115711-1-Si detector) for calibration. The steady state photocurrent generation was measured under the bias of 0.88 V which is a maximum power point of the device with a continuous light illumination for 10 min.

Characterizations: UV–vis–NIR absorption and transmittance spectra were measured using a Varian Cary5000 spectrophotometer. Steady-state PL was observed by Horiba Fluorolog FL-3. Surface morphology of the Cu:NiO_x was investigated using atomic force microscopy in tapping mode and FEI Sirion SEM. XRD was investigated by using X-ray diffractometer (Bruker D8 Discover). XPS was performed by Axis-HSI (Kratos Inc.) at 12 kV and 18 mA with a resolution of 0.1 eV. UPS spectra were obtained on PHI 5000 (ULVAC) using He I emission (21.22 eV). The electrochemical impedance spectroscopy was studied using electrochemical workstation (ESI 600) in the frequency range from 0.1 Hz to 5 MHz under illumination at constant bias of 150 mV. The electrical conductivity of the studied Cu:NiO_x films were measured using a four-point probe station that is connected with a Keithley 2400 source

© 2015 WILEY-VCH Verlag GmbH & Co. KGaA, Weinheim
Adv. Mater. **2015**,
DOI: 10.1002/adma.201503298

meter. The four-point probe with a 100 mm Teflon chuck (0.040 inch spacing) is in line with the specimen. The Cu:NiO_x films were prepared on clean glass substrates.

Supporting Information

Supporting Information is available from the Wiley Online Library or from the author.

Acknowledgements

This work was partially supported by the Office of Naval Research (N00014-14-1-0246), the Department of Energy SunShot (DE-EE0006710), and the Asian Office of Aerospace R&D (FA2386-11-1-4072). A. K.-Y. Jen thanks the Boeing-Johnson Foundation for financial support.

Received: July 8, 2015
Revised: September 11, 2015
Published online:

[1] a) National Renewable Energy Laboratory, http://www.nrel.gov/ncpv/images/efficiency_chart.jpg (accessed: July 2015); b) A. Kojima, K. Teshima, Y. Shirai, T. Miyasaka, *J. Am. Chem. Soc.* **2009**, *131*, 6050; c) G. Xing, N. Mathews, S. Sun, S. S. Lim, Y. M. Lam, M. Grätzel, S. Mhaisalkar, T. C. Sum, *Science* **2013**, *342*, 344; d) S. D. Stranks, G. E. Eperon, G. Grancini, C. Menelaou, M. J. P. Alcocer, T. Leijtens, L. M. Herz, A. Petrozza, H. J. Snaith, *Science* **2013**, *342*, 341; e) J. H. Heo, S. H. Im, J. H. Noh, T. N. Mandal, C.-S. Lim, J. A. Chang, Y. H. Lee, H.-j. Kim, A. Sarkar, M. K. Nazeeruddin, M. Grätzel, S. I. Seok, *Nat. Photonics* **2013**, *7*, 486; f) N. J. Jeon, J. H. Noh, W. S. Yang, Y. C. Kim, S. Ryu, J. Seo, S. I. Seok, *Nature* **2015**, *517*, 476.

[2] a) S. Sun, T. Salim, N. Mathews, M. Duchamp, C. Boothroyd, G. Xing, T. C. Sum, Y. M. Lam, *Energy Environ. Sci.* **2014**, *7*, 399; b) Q. Wang, Q. Dong, Z. Xiao, Y. Yuan, J. Huang, *Energy Environ. Sci.* **2014**, *7*, 2359; c) Z. Xiao, C. Bi, Y. Shao, Q. Dong, Q. Wang, Y. Yuan, C. Wang, Y. Gao, J. Huang, *Energy Environ. Sci.* **2014**, *7*, 2619.

[3] a) Q. Lin, A. Armin, R. C. R. Nagiri, P. L. Burn, P. Meredith, *Nat. Photonics* **2015**, *9*, 106; b) J.-S. Yeo, R. Kang, S. Lee, Y.-J. Jeon, N. Myoung, C.-L. Lee, D.-Y. Kim, J.-M. Yun, Y.-H. Seo, S.-S. Kim, S.-I. Na, *Nano Energy* **2015**, *12*, 96; c) Q. Wang, C. B. J. Huang, *Nano Energy* **2015**, *12*, 275.

[4] a) Z. Xiao, Q. Dong, C. Bi, Y. Shao, Y. Yuan, J. Huang, *Adv. Mater.* **2014**, *26*, 6503; b) J. Seo, S. Park, Y. C. Kim, N. J. Jeon, J. H. Noh, S. C. Yoon, S. I. Seok, *Energy Environ. Sci.* **2014**, *7*, 2642; c) J. A. Christians, R. C. M. Fung, P. V. Kamat, *J. Am. Chem. Soc.* **2013**, *136*, 758; d) S. Ito, S. Tanaka, H. Vahlman, H. Nishino, K. Manabe, P. Lund, *ChemPhysChem* **2014**, *15*, 1194; e) P. Qin, S. Tanaka, S. Ito, N. Tetreault, K. Manabe, H. Nishino, M. K. Nazeeruddin, M. Grätzel, *Nat. Commun.* **2014**, *5*, 3834.

[5] a) J. Y. Jeng, Y. F. Chiang, M. H. Lee, S. R. Peng, T. F. Guo, P. Chen, T. C. Wen, *Adv. Mater.* **2013**, *25*, 3727; b) J. W. Jung, S. T. Williams, A. K.-Y. Jen, *RSC Adv.* **2014**, *4*, 62971; c) J. H. Heo, H. J. Han, D. Kim, T. K. Ahn, S. H. Im, *Energy Environ. Sci.* **2015**, *8*, 1602.

[6] a) A. S. Subbiah, A. Halder, S. Ghosh, N. Mahuli, G. Hodes, S. K. Sarkar, *J. Phys. Chem. Lett.* **2014**, *5*, 1748; b) K.-C. Wang, J.-Y. Jeng, P.-S. Shen, Y.-C. Chang, E. W.-G. Diau, C.-H. Tsai, T.-Y. Chao, H.-C. Hsu, P.-Y. Lin, P. Chen, T.-F. Guo, T.-C. Wen, *Sci. Rep.* **2014**, *4*, 4754; c) C.-C. Chueh, C.-Z. Li, A. K.-Y. Jen, *Energy Environ. Sci.* **2015**, *8*, 1160; d) P. Docampo, J. M. Ball, M. Darwich, G. E. Eperon, H. J. Snaith, *Nat. Commun.* **2013**, *4*, 2761; e) J. W. Jung, C.-C. Chueh, A. K.-Y. Jen, *Adv. Energy Mater.* **2015**, *5*, 1500486.

[7] a) M. D. Irwin, B. Buchholz, A. W. Hains, R. P. H. Chang, T. J. Marks, *Proc. Natl. Acad. Sci. USA* **2008**, *105*, 2783; b) J. R. Manders, S.-W. Tsang, M. J. Hartel, T.-H. Lai, S. Chen, C. M. Amb, J. R. Reynolds, F. So, *Adv. Funct. Mater.* **2013**, *23*, 2993; c) J. Y. Jeng, Y. F. Chiang, M. H. Lee, S. R. Peng, T. F. Guo, P. Chen, T.-C. Wen, *Adv. Mater.* **2013**, *25*, 3727; d) Z. Zhu, Y. Bai, T. Zhang, Z. Liu, X. Long, Z. Wei, Z. Wang, L. Zhang, J. Wang, F. Yan, S. Yang, *Angew. Chem. Int. Ed.* **2014**, *53*, 1; e) L. Hu, J. Peng, W. Wang, Z. Xia, J. Yuan, J. Lu, X. Huang, W. Ma, H. Song, W. Chen, Y.-B. Cheng, J. Tang, *ACS Photon.* **2014**, *1*, 547; f) K.-C. Wang, P.-S. Shen, M.-H. Li, S. Chen, M.-W. Lin, P. Chen, T.-F. Guo, *ACS Appl. Mater. Interface* **2014**, *6*, 11851; g) J. Y. Jeng, K. C. Chen, T. Y. Chiang, P. Y. Lin, T. D. Tsai, Y. C. Chang, T. F. Guo, P. Chen, T. C. Wen, Y. J. Hsu, *Adv. Mater.* **2014**, *24*, 4107.

[8] J. H. Kim, P. W. Liang, S. T. Williams, N. Cho, C. C. Chueh, M. S. Glaz, D. S. Ginger, A. K. Jen, *Adv. Mater.* **2015**, *27*, 695.

[9] a) A. G. Merzhanov, *J. Mater. Chem.* **2004**, *14*, 1779; b) K. Deshpande, A. Mukasyan, A. Varma, *Chem. Mater.* **2004**, *16*, 4896; c) M. Epifani, E. Melissano, G. Pace, M. Schioppa, *J. Eur. Ceram. Soc.* **2007**, *27*, 115.

[10] a) Y. S. Rim, H. S. Lim, H. J. Kim, *ACS Appl. Mater. Interfaces* **2013**, *5*, 3565; b) J. W. Hennek, J. Smith, A. Yan, M.-G. Kim, W. Zhao, V. P. Dravid, A. Facchetti, T. J. Marks, *J. Am. Chem. Soc.* **2013**, *135*, 10729; c) X. Yu, J. Smith, N. Zhou, L. Zeng, P. Guo, Y. Xia, A. Alvarez, S. Aghion, H. Lin, J. Yu, R. P. H. Chang, M. J. Bedzyk, R. Ferragut, T. J. Marks, A. Facchetti, *Proc. Natl. Acad. Sci. USA* **2015**, *112*, 3217.

[11] M.-G. Kim, M. G. Kanatzidis, A. Facchetti, T. J. Marks, *Nat. Mater.* **2011**, *10*, 382.

[12] a) C. Yao, X. Xu, J. Wang, L. Shi, L. Li, *ACS Appl. Mater. Interfaces* **2013**, *5*, 1100; b) S. Bai, M. Cao, Y. Jin, X. Dai, X. Liang, Z. Ye, M. Li, J. Cheng, X. Xiao, Z. Wu, Z. Xia, B. Sun, E. Wang, Y. Mo, F. Gao, F. Zhang, *Adv. Energy Mater.* **2014**, *4*, 1301460.

[13] a) S. T. Williams, C.-C. Chueh, A. K.-Y. Jen, *Small* **2015**, *26*, 3088; b) P.-W. Liang, C.-Y. Liao, C.-C. Chueh, F. Zuo, S. T. Williams, X.-K. Xin, J. Lin, A. K.-Y. Jen, *Adv. Mater.* **2014**, *26*, 3748.

[14] N. J. Jeon, J. H. Noh, Y. C. Kim, W. S. Yang, S. Ryu, S. I. Seok, *Nat. Mater.* **2014**, *13*, 897.

[15] P. W. Liang, C. C. Chueh, S. T. Williams, A. K. Y. Jen, *Adv. Energy Mater.* **2015**, *5*, 1402321.

[16] a) Q. Wang, J.-E. Moser, M. Grätzel, *J. Phys. Chem. B* **2005**, *109*, 14945; b) G. Garcia-Belmonte, P. P. Boix, J. Bisquert, M. Sessolo, H. J. Bolink, *Sol. Energy Mater. Sol. Cells* **2010**, *94*, 366; c) H.-S. Kim, J.-W. Lee, N. Yantara, P. P. Boix, S. A. Kulkarni, S. Mhaisalkar, M. Grätzel, N.-G. Park, *Nano Lett.* **2013**, *13*, 2412; d) E. J. Juarez-Perez, M. Wußler, F. Fabregat-Santiago, K. Lakus-Wollny, *J. Phys. Chem. Lett.* **2014**, *5*, 680; e) L. Liu, A. Mei, T. Liu, P. Jiang, Y. Sheng, L. Zhang, H. Han, *J. Am. Chem. Soc.* **2015**, *137*, 1790.

[17] a) H. J. Snaith, A. Abate, J. M. Ball, G. E. Eperon, T. Leijtens, N. K. Noel, S. D. Stranks, J. T.-W. Wang, K. Wojciechowski, W. Zhang, *J. Phys. Chem. Lett.* **2014**, *5*, 1511; b) Z. Xiao, C. Bi, Y. Shao, Q. Dong, Q. Wang, Y. Yuan, C. Wang, Y. Gao, J. Huang, *Energy Environ. Sci.* **2014**, *7*, 2619; c) E. L. Unger, E. T. Hoke, C. D. Bailie, W. H. Nguyen, A. R. Bowring, T. Heumüller, M. G. Christoforod, M. D. McGehee, *Energy Environ. Sci.* **2014**, *7*, 3690; d) Z. Xiao, Y. Yuan, Y. Shao, Q. Wang, Q. Dong, C. Bi, P. Sharma, A. Gruverman, J. Huang, *Nat. Mater.* **2015**, *14*, 193; e) W. Tress, N. Marinova, T. Moehl, S. M. Zakeeruddin, M. K. Nazeeruddin, M. Grätzel, *Energy Environ. Sci.* **2015**, *8*, 995.

© 2015 WILEY-VCH Verlag GmbH & Co. KGaA, Weinheim